Optimization of Enzyme Mechanism along the Evolutionary Trajectory of a Computationally Designed (Retro-)Aldolase

Originally published in:
Journal of the American Chemical Society 139(36), https://doi.org/10.1021/jacs.7b05796

Optimization of Enzyme Mechanism along the Evolutionary Trajectory of a Computationally Designed (Retro-)Aldolase

Cathleen Zeymer, Reinhard Zschoche, and Donald Hilvert*

Laboratory of Organic Chemistry, ETH Zürich, 8093 Zürich, Switzerland

ABSTRACT: *De novo* biocatalysts have been successfully generated by computational design and subsequent experimental optimization. Here, we examined the evolutionary history of the computationally designed (retro-)aldolase RA95. The modest activity of the starting enzyme was previously improved 10^5 fold over many rounds of mutagenesis and screening to afford a proficient biocatalyst for enantioselective cleavage and synthesis of β-hydroxyketones. Using a set of representative RA95 variants, we probed individual steps in the multistep reaction pathway to determine which processes limit steady-state turnover and how mutations that accumulated along the evolutionary trajectory influenced the kinetic mechanism. We found that the overall rate-limiting step for aldol cleavage shifted from C-C bond scission (or an earlier step in the pathway) for the computational design to product release for the evolved enzymes. Specifically, interconversion of Schiff base and enamine intermediates, formed covalently between acetone and the catalytic lysine residue, was found to be the slowest step for the most active variants. A complex hydrogen bond network of four active site residues, which was installed in the late stages of laboratory evolution, apparently enhances lysine reactivity and facilitates efficient proton shuffling. This catalytic tetrad accounts for the tremendous rate acceleration observed for all steps of the mechanism, most notably Schiff base formation and hydrolysis. Comparison of our results with kinetic and structural studies on natural aldolases provides valuable feedback for computational enzyme design and laboratory evolution approaches alike.

INTRODUCTION

Combining computational enzyme design with laboratory evolution has proven to be a successful strategy for developing novel biocatalysts with non-natural function,[1,2] such as Kemp eliminases[3-6] and Diels-Alderases.[7,8] Monitoring the evolutionary history of such systems has the potential to provide valuable insights into both enzyme mechanism and the basic principles of molecular evolution. One class of *de novo* protein catalysts, namely the (retro-)aldolases, is particularly well suited for this kind of retrospective study, as successful designs are available in multiple protein scaffolds.[9-11] Because the aldol reaction proceeds via a multistep mechanism involving several covalent intermediates, its analysis can shed light on how complex reaction manifolds adapt to selective evolutionary pressures.

Retro-aldolase RA95, one of the best-studied *de novo* enzymes, was computationally designed to promote carbon-carbon bond cleavage of β-hydroxyketones via amine catalysis. The starting catalyst, RA95.0, which was equipped with a reactive lysine adjacent to a hydrophobic binding pocket (Figure 1), cleaves the abiological aldol substrate methodol with a ca. 10^4-fold rate acceleration over background (k_{cat}/K_M = 0.17 M^{-1} s^{-1}).[9,10] It was subsequently improved >9000 fold over many rounds of mutagenesis and medium-throughput screening in microtiter plates to give variant RA95.5-8 (k_{cat}/K_M = 1,600 M^{-1} s^{-1}).[10,12] Optimization entailed substantial structural rearrangements at the active site, including complete replacement of the originally designed catalytic apparatus. Further evolution using fluorescence-activated droplet sorting (FADS), a microfluidic-based ultrahigh-throughput screening technique,[13-15] yielded variant RA95.5-8F (k_{cat}/K_M = 34,000 M^{-1} s^{-1}).[16] This highly active enzyme possesses an active site with a sophisticated hydrogen bond network of catalytic residues, reminiscent of the functional group arrays in natural class I aldolases.[16,17] RA95.5-8F not only exhibits a $>10^9$-fold rate acceleration over uncatalyzed methodol cleavage, it is also an efficient and highly enantioselective catalyst for the synthesis of aldol products.[16] As such, it may be useful for the stereospecific formation of C-C bonds in diverse high-value compounds.[18]

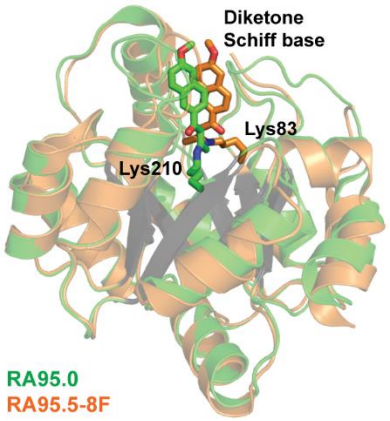

Figure 1. The computationally designed retro-aldolase RA95 before (RA95.0, green, PDB code: 4A29) and after laboratory evolution (RA95.5-8F, orange, PDB code: 5AN7) in complex with a mechanism-based diketone inhibitor. Although the overall structure of the TIM barrel scaffold did not change, active site and substrate binding pocket were remodeled substantially, including a change in the position of the catalytic lysine residue.[12,16]

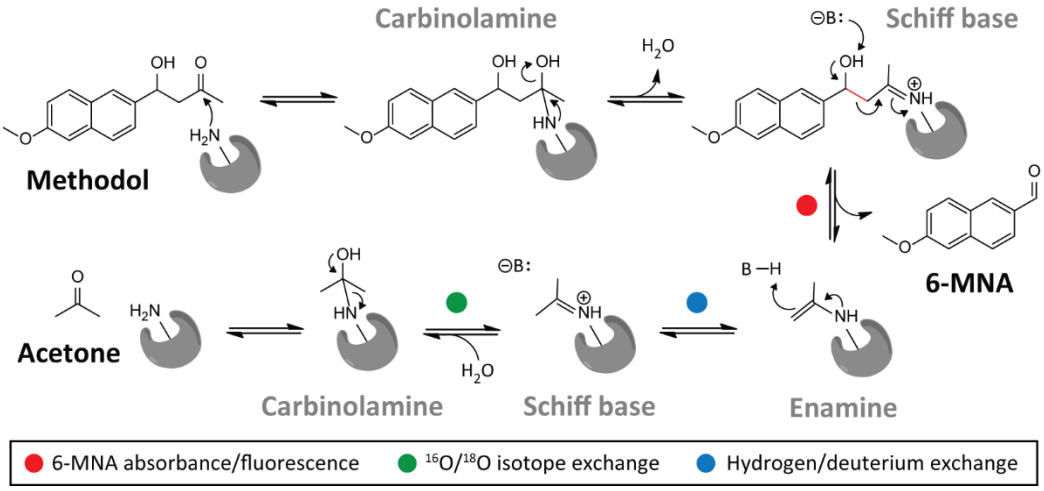

Figure 2. The multistep (retro-)aldolase mechanism. The colored circles indicate the individual steps of the mechanism that were probed by different enzyme kinetics experiments. Red: C-C bond cleavage and formation were monitored by 6-MNA absorbance and fluorescence under steady state and single turnover conditions. Green: Schiff base formation and hydrolysis were monitored by oxygen isotope exchange. Blue: Enamine formation was monitored by hydrogen/deuterium exchange.

Exploiting the broad scope of amine catalysis, RA95 variants have also been applied to a range of other transformations that proceed via reactive enamine and iminium ion intermediates, including Michael additions, Knoevenagel condensations and Henry reactions.[19-21]

The current study was motivated by the belief that understanding the factors that promote high catalytic efficiency in these *de novo* biocatalysts could help to improve computational design protocols as well as refine experimental optimization strategies. We thus focused on dissecting what happened mechanistically along the RA95 evolutionary trajectory. What was the rate-limiting step in the aldol cleavage mechanism initially and did it change as the enzyme was optimized? Did elementary steps in the pathway respond uniformly or differentially to mutation? Which modifications enabled effective catalysis of aldol synthesis? To address these questions, we probed specific steps of the aldolase reaction pathway kinetically, as depicted in Figure 2, and compared our findings directly with mechanistic studies of natural aldolases. Our results contribute to a deeper understanding of the aldolase mechanism and reveal how directed evolution gradually reshaped the complex reaction profile to optimize catalytic efficiency.

RESULTS

Preparation and Steady-State Characterization of RA95 Variants. We chose the starting computational design RA95.0 and the evolved variants RA95.5-8 and RA95.5-8F for detailed mechanistic investigation. These proteins, which have been kinetically and structurally characterized,[10,12,16] were produced and purified as previously described, and the reported steady-state parameters for methodol cleavage were confirmed with minor batch-to-batch variation (Table 1). RA95.0, which exhibits modest (*S*)-selectivity, was assayed with enantiopure (*S*)-methodol, whereas enantiopure (*R*)-methodol was used for all measurements with the (*R*)-selective RA95.5-8 and RA95.5-8F variants. As outlined below, we utilized pre-steady-state kinetic methods and isotope exchange experiments to dissect the key steps in the aldol reaction pathway (Figure 2). Comparison of the collected rate constants with the steady-state turnover numbers (k_{cat}), which report on the slowest step(s) in the aldol cleavage mechanism, allow us to assess which microscopic processes limit these catalysts. Such experiments also provide valuable insights into how mutations that arose during evolutionary optimization influenced the kinetic mechanism.

Single-Turnover Measurements. We first investigated the rate of the C-C bond cleavage step. High enzyme concentrations, well in excess over substrate and, if possible, significantly higher than the K_D value for methodol, were used to guarantee only a single catalytic turnover per active site. The measurements were performed by rapid mixing of enzyme and methodol in a stopped flow apparatus, monitoring the increase in fluorescence due to formation of the product 6-methoxy-2-naphthaldehyde (6-MNA) as a function of increasing catalyst concentration.

The single turnover rate constant (k_{ST}) for the original computational design, RA95.0, is 1.1 x 10^{-4} s^{-1} (Figure S1). This value is the same as the k_{cat} for (*S*)-methodol cleavage by this enzyme, indicating that C-C bond scission or an earlier step in the aldol cleavage mechanism must be rate limiting for the starting catalyst. Brønsted values determined for non-enzymatic retro-aldol cleavage of methodol catalyzed by small organic amines have suggested that cleavage of the C-C bond rather than iminium ion formation likely limits the reaction rates for these simple systems.[22] Although mechanistic differences are conceivable, a common rate-determining step for the enzymatic and amine-catalyzed transformations seems plausible considering the highly solvated RA95.0 active site.[12]

The k_{ST} values determined for RA95.5-8 and RA95.5-8F are respectively >6 x 10^3 and 3 x 10^5 times higher than the k_{ST} for RA95.0, highlighting the extent to which C-C bond scission was accelerated over the course of experimental evolution. Because these rate constants also exceed the turnover numbers of these enzymes by roughly a factor of 5 (Figure 3A and Table 1), cleavage of the C-C bond (and all previous steps in the pathway) cannot be rate determining overall. A later process associated with product release must therefore limit catalysis by the evolved variants. Screening of mutant libraries for more efficient catalysts evidently shifted the kinetic bottleneck for retro-aldol cleavage to a later step in the reaction pathway.

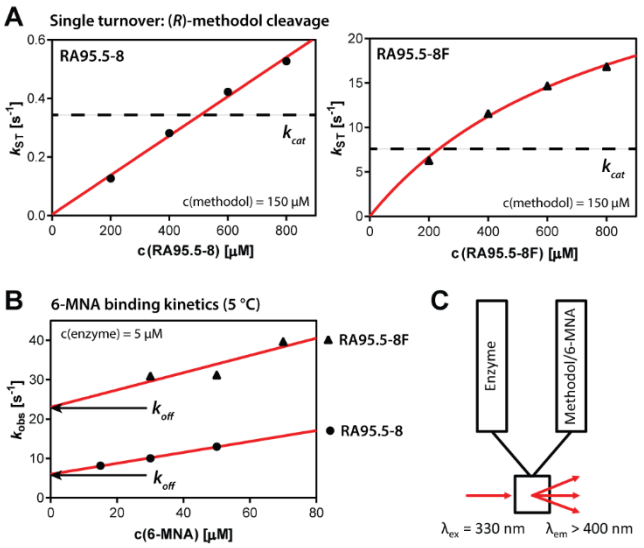

Figure 3. Stopped flow kinetics. (*R*)-Methodol cleavage under single turnover conditions (A) and 6-MNA binding kinetics (B) were measured with the same stopped flow setup (C). The kinetic parameters obtained from these experiments are listed in Table 1.

6-MNA Binding and Dissociation Are Fast Processes. Methodol cleavage yields two products, acetone and 6-MNA. Whereas acetone release from the enzyme occurs over several steps via distinct covalent intermediates (enamine to Schiff base to carbinolamine), 6-MNA dissociates in a single step. We measured the binding kinetics of 6-MNA in a stopped-flow experiment (Figure 3B and Table 1). The change in 6-MNA fluorescence upon binding to the enzyme was monitored at different concentrations of 6-MNA. Single exponential kinetic traces were obtained, and the fitted rate constants show a linear dependence on 6-MNA concentration, allowing estimation of the dissociation rate constant (k_{off}) from the y-axis intercept. Because the binding transitions are very fast, measurements were performed at low temperature (5 °C). The rates at 29 °C, the temperature used for all other kinetic measurements, are expected to be about four times higher. Although the rate constants were determined in the absence of acetone, which might influence binding to some extent, and formation of some covalent 6-MNA-enzyme adducts[10,22] cannot be ruled out, the data show that 6-MNA association is quite rapid ($k_{on,5°C} > 10^5$ M^{-1} s^{-1}), and that dissociation ($k_{off,5°C}$ = 6 and 23 s^{-1} for RA95.5-8 and RA95.5-8F, respectively) is considerably faster than steady-state methodol cleavage. Thus, 6-MNA release can be excluded as the rate-determining step for the retro-aldol reaction under steady-state conditions, indicating that one of the steps associated with acetone release must limit overall turnover of the improved enzymes. Comparatively rapid 6-MNA release can be rationalized by the structures of RA95.5-8 and RA95.5-8F, which show that the acetone binding site is more deeply buried than the apolar pocket that accommodates 6-MNA.[12,16]

Directed Evolution Greatly Accelerates Schiff Base Formation and Hydrolysis. We used an oxygen isotope exchange experiment to probe formation and hydrolysis of the covalent Schiff base intermediate formed between acetone and the catalytic lysine. The evolved RA95 variants were incubated with various concentrations of ^{16}O-acetone in $H_2{}^{18}O$ buffer, and the rates of ^{18}O-acetone accumulation were measured with a GC-MS instrument and fitted to the Michaelis-Menten equation (Figure 4A and Table 1). Under saturating conditions, the exchange rate constants (k_{ex}) were 2.7 s^{-1} for RA95.5-8 and 330 s^{-1} for RA95.5-8F, which are substantially (8- and 45-fold) larger than the respective k_{cat} values for methodol cleavage. Thus, hydrolysis of the Schiff base during acetone release cannot be rate limiting for either retro-aldolase.

The 300-fold increase in k_{ex}/K_M for RA95.5-8F compared to RA95.5-8 is particularly notable in this context, underscoring the importance of mutations introduced in the last stages of optimization for enhancing the efficiency of Schiff base formation and hydrolysis (via a carbinolamine intermediate).

Conversion of the Enamine and Schiff Base Intermediates Is Slow. Having eliminated all plausible alternatives, the only remaining step in the retro-aldol reaction pathway, namely protonation of the enamine to give the Schiff base between acetone and the catalytic lysine, must be rate limiting overall. Because interconversion of the enamine and Schiff

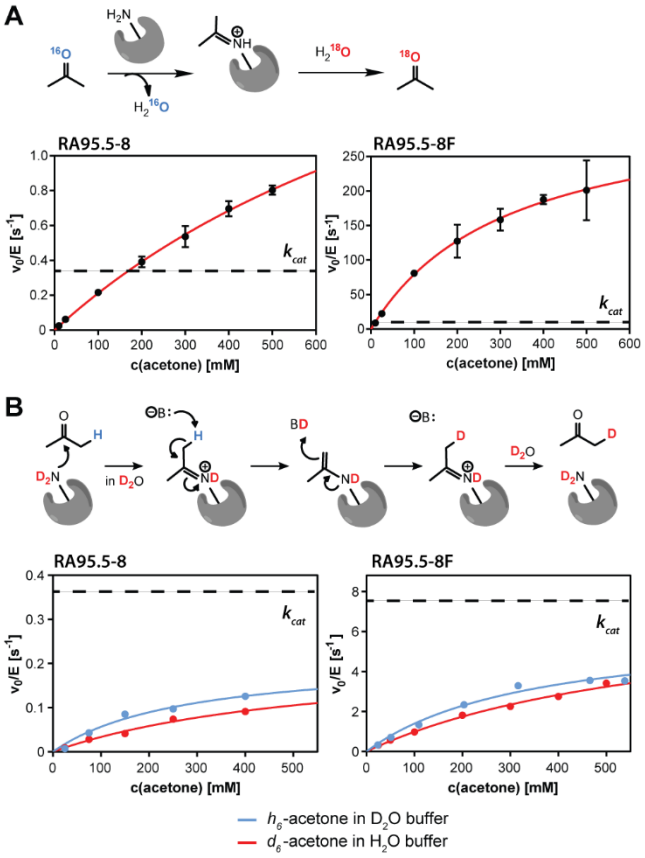

Figure 4. Isotope exchange kinetics. (A) ^{16}O/^{18}O isotope exchange kinetics measurement probing the formation and hydrolysis of the Schiff base intermediate formed from acetone. For both RA95.5-8 and RA95.5-8F, the Schiff base formation/hydrolysis is significantly faster than steady-state (*R*)-methodol cleavage (k_{cat} is indicated by the dotted line). (B) Hydrogen/deuterium exchange kinetics measurement probing the formation of the enamine intermediate formed from acetone. The exchange rate constant k_{ex} for both RA95.5-8 and RA95.5-8F is 30-40 % lower than k_{cat} for methodol cleavage (dotted line). The kinetic parameters obtained from these experiments are listed in Table 1.

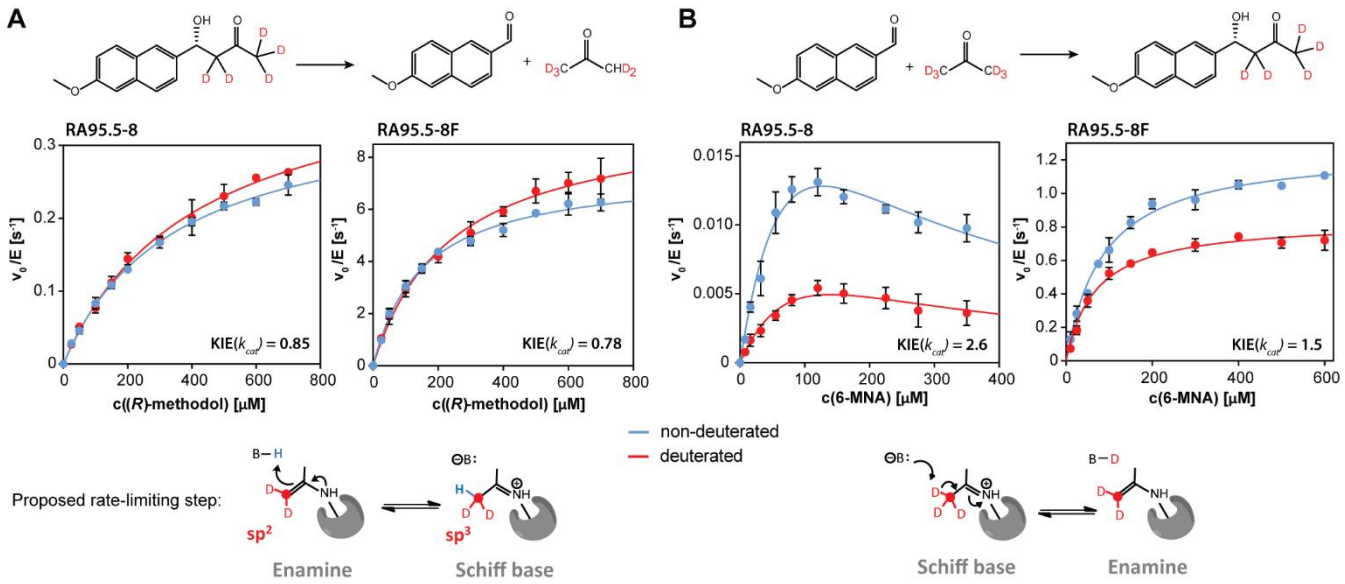

Figure 5. Kinetic isotope effects (KIEs). (A) (*R*)-Methodol cleavage under steady state conditions. Deuterated (red) and non-deuterated (blue) (*R*)-methodol were used as substrates for RA95.5-8 and RA95.5-8F in order to determine secondary KIEs. An inverse secondary KIE was found for k_{cat}. (B) Methodol synthesis from 6-MNA and fully deuterated (red) or non-deuterated (blue) acetone under steady state conditions. The concentration of acetone was kept constant at 1.0 M, whereas c(6-MNA) was varied. Here, KIEs are 2.6 and 1.5 for RA95.5-8 and RA95.5-8F, respectively. Because RA95.5-8 exhibits strong substrate inhibition and cannot be saturated with acetone, the k_{cat} for methodol synthesis is substantially underestimated in this case. The kinetic parameters obtained from these experiments are summarized in Table 1.

base intermediates occurs via acid/base-catalyzed protonation/deprotonation, we used an NMR-based hydrogen/deuterium exchange experiment to probe this step. RA95.5-8 and RA95.5-8F were incubated with h_6-acetone in D_2O buffer and the formation of mono-deuterated h_5,d_1-acetone was measured by ^{1}H-NMR spectroscopy (Figure 4B and Table 1). In complementary experiments, the enzymes were incubated with fully deuterated d_6-acetone in H_2O buffer and ^{2}H-NMR spectroscopy was used to monitor formation of h_1,d_5-acetone. In both cases, the H/D exchange rate constants k_{ex} were 30-40% lower than k_{cat} for methodol cleavage for both RA95.5-8 and RA95.5-8F. This result, together with the fact that all other steps were found to be faster than k_{cat} and therefore not rate-limiting, supports the inference that protonation of the enamine during acetone release is the step in the cleavage pathway that limits the turnover efficiency of both catalysts.

To provide additional evidence for this hypothesis, we determined the secondary kinetic isotope effect (KIE) for methodol cleavage under steady-state conditions using non-deuterated and partially deuterated methodol as substrates (Figure 5A and Table 1). The requisite d_5-(*R*)-methodol was synthesized enzymatically from d_6-acetone and 6-MNA in D_2O buffer using RA95.5-8F as a catalyst. Steady-state measurements yielded an inverse secondary deuterium KIE on k_{cat} of ~0.8 for both RA95.5-8 and RA95.5-8F, implicating a rate-limiting process in which an sp^2-hybridized carbon atom is converted into an sp^3 center. Protonation of the enamine intermediate is the only such transformation in the cleavage pathway (Figure 2). If C-C bond scission of methodol to form the enamine were rate limiting, a normal KIE > 1 would have been expected, as this step is associated with an sp^3 to sp^2 hybridization change. Thus, we can conclude that conversion of the enamine into the Schiff base intermediate during acetone release dictates the rate of methodol cleavage catalyzed by RA95.5-8 and RA95.5-8F. An ordered water molecule, bound by polar residues proximal to the enamine intermediate,[16] is a possible source of the respective proton.

Aldol Synthesis. From a synthetic point of view, the formation of enantiopure β-hydroxyketones is more valuable than their cleavage. However, methodol synthesis from 6-MNA and acetone was not possible with the original computationally designed aldolases, including RA95.0. Because the synthetic reaction is a bimolecular process that is thermodynamically unfavorable, high acetone concentrations are required to push the equilibrium toward the aldol product. Unfortunately, the original designs do not tolerate large amounts of organic co-solvent. Even more problematic, 6-MNA is a better electrophile than acetone and inhibits the enzyme by forming a covalent Schiff base adduct with the catalytic lysine[10,22], thus blocking the active site.

Both obstacles were gradually overcome by directed evolution. The intermediate RA95.5-8 variant, for example, catalyzes the formation of significant amounts of methodol from 6-MNA and acetone. Nevertheless, its affinity for acetone is too low ($K_D \approx 1$ M) to saturate the enzyme under practical experimental conditions, and substantial substrate inhibition by 6-MNA is still observed (Figure 5B). These features prevent RA95.5-8 from being a synthetically useful catalyst for aldol synthesis. They also complicate kinetic analysis of the synthetic reaction, thwarting efforts to determine the true k_{cat} for methodol formation at saturating acetone concentrations.

In contrast, structural and mechanistic modifications introduced in the late stages of evolution make RA95.5-8F an excellent aldolase. The 3-fold increase in apparent affinity for acetone allows saturation of the enzyme without co-solvent-induced losses in activity, and steady-state kinetics measured at 1 M acetone show no sign of substrate inhibition by 6-MNA

(Figure 5B). Both of these properties are byproducts of ultra-high-throughput screening for mutations that maximized the amount of product formed in a given time interval, thus simultaneously optimizing total turnover number and initial rates of product formation. As a consequence, RA95.5-8F catalyzes the addition of acetone to a broad range of functionalized aromatic and aliphatic aldehydes, affording useful conversions and good-to-excellent enantioselectivities.[16]

Although the affinity for acetone increased over the course of evolution, the K_D value for this substrate is still high, precluding true single turnover conditions even with the most active variant. As a result, an unambiguous assignment of the overall rate-limiting step for the synthetic reaction is not possible. Nevertheless, we determined steady-state KIEs for methodol synthesis using 1 M deuterated and non-deuterated acetone as substrates (Figure 5B and Table 1). Primary KIEs on k_{cat} for RA95.5-8 and RA95.5-8F are 2.6 and 1.5, respectively, indicating that cleavage of a C-H/D bond is at least partially rate limiting under these conditions. The only deprotonation step in the synthetic direction is the conversion of the acetone Schiff base into the corresponding enamine (Figure 2), i.e. the reverse of the step that limits enzyme-catalyzed aldol cleavage. However, because the H/D exchange rate constants for enamine formation are still higher than the k_{cat} values measured for methodol synthesis, a later step, either C-C bond formation or methodol release, must partially limit aldol synthesis

Table 1. Enzyme kinetic parameters[a]

	RA95.5-8	RA95.5-8F
(*R*)-Methodol cleavage		
- Steady state		
Non-deuterated	k_{cat} = 0.36 ± 0.01 s^{-1} K_M = 346 ± 20 µM	k_{cat} = 7.5 ± 0.2 s^{-1} K_M = 153 ± 11 µM
Deuterated	k_{cat} = 0.42 ± 0.02 s^{-1} K_M = 418 ± 40 µM	k_{cat} = 9.7 ± 0.4 s^{-1} K_M = 240 ± 23 µM
- KIE	KIE(k_{cat}) = 0.85	KIE(k_{cat}) = 0.78
- Single turnover	k_{ST} >> 0.6 s^{-1}	k_{ST} = 35 ± 4 s^{-1}
6-MNA binding (at 5°C)		
	k_{on} = (1.4 ± 0.1) x 10^5 M^{-1} s^{-1} k_{off} = 6.0 ± 0.3 s^{-1}	k_{on} = (2.2 ± 1.2) x 10^5 M^{-1} s^{-1} k_{off} = 23 ± 6 s^{-1}
Schiff base formation ($^{16}O/^{18}O$ isotope exchange)		
^{16}O-acetone in $H_2{}^{18}O$	k_{ex} = 2.7 ± 0.6 s^{-1} K_M = 1200 ± 340 mM	k_{ex} = 330 ± 50 s^{-1} K_M = 320 ± 90 mM
Enamine formation (H/D isotope exchange)		
h_6-acetone in D_2O	k_{ex} = 0.21 ± 0.05 s^{-1} K_M = 280 ± 112 mM	k_{ex} = 5.2 ± 0.5 s^{-1} K_M = 270 ± 60 mM
d_6-acetone in H_2O	k_{ex} = 0.23 ± 0.06 s^{-1} K_M = 575 ± 240 mM	k_{ex} = 7.6 ± 1.8 s^{-1} K_M = 670 ± 230 mM
Methodol synthesis[b]		
- Steady state		
Non-deuterated acetone	k_{cat} = 0.038 ± 0.001 s^{-1} K_M = K_i = 128 ± 6 µM	k_{cat} = 1.3 ± 0.03 s^{-1} K_M = 87 ± 7 µM
Deuterated acetone	k_{cat} = 0.015 ± 0.001 s^{-1} K_M = K_i = 140 ± 11 µM	k_{cat} = 0.84 ± 0.02 s^{-1} K_M = 68 ± 6 µM
- KIE	KIE(k_{cat}) = 2.6	KIE(k_{cat}) = 1.5

[a] If not indicated otherwise, all measurements were performed at 29 °C in 25 mM HEPES buffer (pH 7.5) containing 150 mM NaCl.

[b] Steady-state data measured at constant c(acetone) = 1 M. K_m and K_i refer to 6-MNA, which was varied in concentration.

DISCUSSION

Natural class I aldolases like fructose-1,6-diphosphate (FDP) aldolase, a key enzyme in glucose metabolism, employ a multistep pathway involving amine catalysis and enzyme-bound Schiff base intermediates to convert substrates to products.[17] In addition to a catalytic lysine, their active sites contain extensive arrays of functional groups that mediate substrate binding, transition state stabilization, and essential proton transfers during catalysis. Mechanistic studies on FDP aldolase have shown that neither Schiff base formation/hydrolysis nor C-C bond formation/cleavage is rate limiting. Instead, the slowest steps for both FDP cleavage and synthesis are associated with product release.[23-27]

In an attempt to mimic the properties of such enzymes, computational methods have been used to install reactive lysines in a variety of natural protein scaffolds.[9-11] Enzymes that accelerate the retro-aldol cleavage of methodol have been successfully produced in this way, but their activities are low (k_{cat}/K_M < 1 M^{-1} s^{-1}) compared to natural aldolases (k_{cat}/K_M = 10^5 to 10^6 M^{-1} s^{-1}). Investigations of RA61, one of the most active original designs, have suggested that most of the enzyme's 10^5-fold rate acceleration can be attributed to the positioning of the substrate in a hydrophobic binding pocket proximal to a lysine with a reduced pK_a.[22] Although most designs also included a catalytic water molecule oriented by polar residues to facilitate proton transfers, mutagenesis studies have shown that this element generally does not contribute to catalytic efficiency.[22]

Like other computationally designed retro-aldolases, RA95.0 was equipped with a simple catalytic motif consisting of a reactive lysine (Lys210) to activate the substrate by Schiff base formation and a glutamate (Glu53) to position an ordered water molecule for proton transfer. As for RA61, though, targeted mutagenesis showed that the latter feature does not play a role in catalysis.[12] Analysis of the subsequent evolutionary trajectory of this catalyst suggests that its comparatively low starting activity is due to the absence of additional functional groups in the vicinity of Lys210 that could assist formation and breakdown of the first carbinolamine intermediate or deprotonation of the ensuing Schiff base intermediate to initiate C-C bond scission. Unsurprisingly, turnover is therefore limited by C-C bond cleavage or one of the steps leading up to it, rather than product release as in FDP aldolase.

As the activity of RA95.0 was improved by directed evolution, its active site underwent substantial remodeling. The associated molecular changes enabled increasingly precise molecular recognition, as evidenced by a steady increase in enantiospecificity (the specificity for (*R*) over (*S*)-configured methodol increased from 0.4 for the starting design to 14 and 480 for RA95.5-8 and RA95.5-8F, respectively).[16] The crystal structure of RA95.5-8F in complex with a mechanism-based inhibitor revealed that the enzyme, like its natural counterparts, exploits an extensive range of specific polar and apolar interactions to orient the substrate for reaction and discriminate between the competing diasteromeric transition states.[16]

The observed remodeling was not restricted to refining enzyme-substrate complementarity. Complete replacement of the original catalytic apparatus with a more effective constellation of functional groups attests to even more fundamental alterations.[12,16] For example, an alternative lysine residue (Lys83) emerged early in evolution and gradually supplanted the originally designed Lys210. This mechanistic substitution was made possible by the stepwise installation of three supporting polar residues in the vicinity of the new lysine. In the most evolved variant, Tyr51, Asn110 and Tyr180 form a tight hydrogen bond network with Lys83 (Figure 6A), lowering the pK_a of the catalytic lysine to 6.2 and facilitating efficient proton shuffling during catalysis. Surrounding mutations, identified by extensive ultrahigh-throughput screening of large gene libraries in the final rounds of optimization, likely further fine-tuned this catalytic device.

Comparisons of RA95.5-8 and RA95.5-8F show that installation of the Lys-Tyr-Asn-Tyr tetrad improved overall performance substantially, although the elementary steps along the reaction coordinate responded differentially to this evolutionary innovation (Table 1). The >120-fold acceleration of water-acetone oxygen exchange indicates that Schiff base formation and hydrolysis were enhanced to the greatest extent, likely because the transition states for formation and breakdown of the intermediate carbinolamine adduct are particularly well stabilized by this hydrogen bonding network. Similar effects may also be responsible for the improvements seen for the early steps of methodol cleavage, up to and including C-C bond scission (which is likely promoted by either Tyr51 or Tyr180 functioning as a base), rationalizing the shift we observed in overall rate-determining step from aldol cleavage for the computational design to product release for the evolved catalysts.

Judging from the 25-fold increase in the rate of H/D-exchange with acetone catalyzed by RA95.5-8F versus RA95.5-8, the evolved hydrogen bond network also enhanced interconversion of the enamine and Schiff base intermediates, which (partially) limits turnover efficiency in both the cleavage and synthetic directions. Similar effects have been observed previously for both natural aldolases[17] as well as catalytic antibodies.[28] The structure of RA95.5-8F suggests that the catalytic tetrad could position an ordered water/hydroxide molecule that could serve as the acid/base in this step.[16] Rapid formation of the enamine from acetone, of course, is essential for efficient production of aldol products from acetone and aldehydes. In conjunction with the proximal hydrophobic pocket for binding 6-MNA, which was introduced by design and preserved over the entire evolutionary trajectory,[16] efficient deprotonation of the acetone Schiff base intermediate, either directly by one of the polar supporting residues or by a bound hydroxide, accounts for RA95.5-8F's utility as a biocatalyst.

The catalytic tetrad in RA95.5-8F resembles the catalytic machineries found in natural class I aldolases. The structural resemblance with fructose-6-phosphate (F6P) aldolase is particularly striking.[29-31] In addition to the canonical catalytic lysine, the F6P aldolase active site contains a tyrosine and a glutamine—analogous to Tyr51 and Asn110 in the evolved RA95 variants—that position a catalytic water near the covalently bound substrate. The tyrosine in F6P aldolase is also believed to play a multifunctional role as an acid/base in catalysis. In support of this view, homologous transaldolases have been converted into efficient F6P aldolases by replacing a suitably positioned active site phenylalanine with a tyrosine.[32,33] A double mutant containing an additional glutamate-to-glutamine substitution (Figure 6B) was even slightly more active than an authentic F6P aldolase (k_{cat} = 1.3 s^{-1} and k_{cat}/K_M = 108 M^{-1} s^{-1}).[33] Structural and mechanistic studies of the latter variant showed that tyrosine-mediated protonation of the enamine intermediate formed upon F6P cleavage was the rate-limiting step. Thus, the analogy between F6P aldolase and RA95.5-8F extends to kinetic mechanism. Optimization of the computational design over many rounds of laboratory evolution apparently converged on a solution to the problem of catalyzing aldol cleavage and synthesis already known in nature.

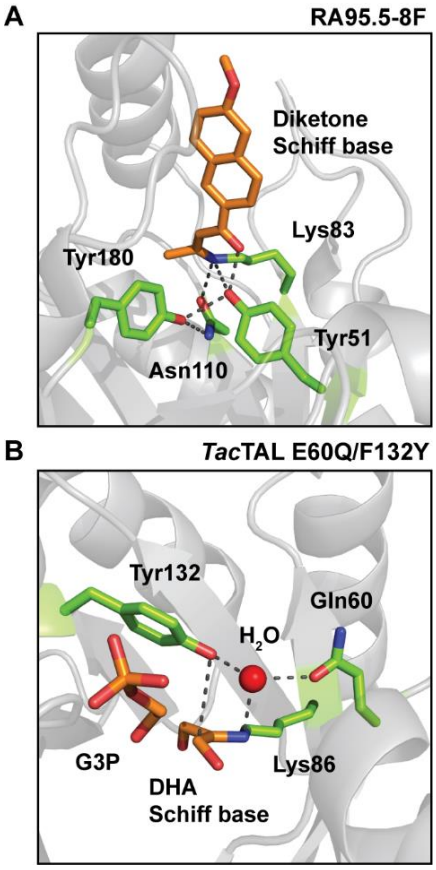

Figure 6. Structural comparison of the catalytic machinery in active aldolases. (A) Structure of RA95.5-8F in complex with a diketone inhibitor, bound covalently as a Schiff base via the catalytic lysine residue. Residues Lys83, Tyr180, Tyr51 and Asn110 form a catalytic tetrad essential for activity. The sophisticated hydrogen bond network between these residues and the substrate is proposed to facilitate efficient protonation/deprotonation. PDB code: 5AN7. (B) Structure of a mutated transaldolase from *Thermoplasma acidophilum.* Mutations in key catalytic residues (E60Q and F132Y) led to a switch from transaldolase to fructose-6-phosphate (F6P) aldolase activity.[33] The protein was co-crystallized with F6P, which was converted to glyceraldehyde-3-phosphate (G3P) and dihydroxy-acetone (DHA), the latter being bound covalently as a Schiff base via the catalytic lysine. The active site arrangement shown here, comprising a tyrosine and a glutamine residue, is proposed to efficiently catalyze the rate-limiting step in aldol cleavage, namely protonation of the carbanion-enamine intermediate, in F6P aldolase. [31,33] PDB code: 4XZ9.

CONCLUSION

In combination with previously available structural data, the current kinetic study has deepened our understanding of the evolutionary transformations that enabled conversion of a mediocre *de novo* aldolase into a proficient enzyme. The mechanistic issues identified by our analysis are likely to be relevant for future efforts to design and evolve protein catalysts with true enzyme-like activities and selectivities.

Looking forward, improved computational and experimental methods to incorporate functional group arrays are clearly needed. The catalytic motifs in first-generation computational designs are relatively simplistic and were installed with insufficient precision to achieve high activity. Observed rate enhancements typically fall in the range 10^2 to 10^4 fold over background,[9,10] far below those observed for natural aldolases. As a consequence, the starting designs require extensive or, as in the case of the RA95 aldolase, complete experimental redesign to achieve practically useful activities. Laboratory evolution has proved to be a particularly powerful tool for augmenting the efficiency of these catalysts, often boosting the activity by an additional three to five orders of magnitude.

Although the prospect of directly designing highly active enzymes is still some way off, recent progress in modeling atomically accurate polar networks[34] is cause for optimism. By installing hydrogen-bond donors and acceptors in the vicinity of key catalytic residues, more effective starting catalysts can be expected. These, in turn, may be easier to optimize by directed evolution, taking advantage of smart libraries[35-37] and ultrahigh-throughput screening modalities[13-15,38-40] to navigate sequence space more effectively.

EXPERIMENTAL SECTION

Materials. All chemicals were purchased from Sigma-Aldrich, Merck or Fluka and used without further purification. Isotopically labeled compounds (D_2O, $H_2{}^{18}O$, NaOD, $CDCl_3$, d_6-acetone, d_3-acetonitrile) were purchased from Cambridge Isotope Laboratories Inc.

Protein Production and Purification. RA95.0, RA95.5-8 and RA95.5-8F were produced in *E. coli* BL21 Gold (DE3) and purified by nickel affinity chromatography as previously described.[12,16] The enzymes were stored in buffer A (25 mM HEPES pH 7.5 and 150 mM NaCl), which was also used for all kinetic assays. The same buffer was prepared in either D_2O (note: pD = pH + 0.4) or $H_2{}^{18}O$ for the respective isotope exchange experiments described below.

Synthesis of Deuterated d_5-(*R*)-Methodol. The enzymatic synthesis of (*R*)-methodol from acetone and 6-MNA using RA95.5-8F as a biocatalyst was reported previously.[16] Here, we used this approach with fully deuterated acetone as the substrate:

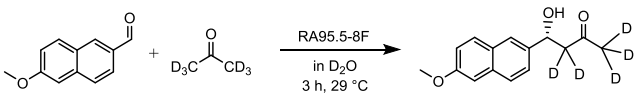

The reaction mixture contained 2 mM 6-MNA, 2 M d_6-acetone and 0.1 µM RA95.5-8F in 50 ml buffer A prepared in D_2O. The mixture was gently shaken for 3 hours at 29 °C, and subsequently saturated with 15 g solid sodium chloride and extracted with 3 x 50 ml ethyl acetate. The organic phase was dried over sodium sulfate before removing the solvent under vacuum. The crude material was purified by flash chromatography. The reaction yielded 11.8 mg d_5-(*R*)-methodol (47% isolated yield). Chiral HPLC analysis was performed as described previously[16] using a Reprosil 100 Chiral-NR column (8 µm, 250 x 4,6 mm) and isocratic hexane/EtOAc = 3:7. The (*R*):(*S*) ratio for the isolated product was 99.3 : 0.7. The deuteration pattern was confirmed by NMR and mass spectrometry by direct comparison with non-deuterated (*R*)-methodol (Figure S2). ^{1}H NMR (300 MHz, $CDCl_3$) δ 7.65 (m, 3H), 7.35 (dd, 1H), 7.07 (m, 2H), 5.20 (d, 1H), 3.84 (s, 3H), 3.25 (d, 1H). ^{13}C NMR (101 MHz, $CDCl_3$) δ 209.42, 157.75, 137.81, 134.12, 129.45, 128.74, 127.21, 124.28, 119.06, 105.67, 77.20, 69.93, 55.31. HRMS (ESI): calculated for $[C_{15}H_{11}D_5O_3]^+$: m/z = 249.1413, found: m/z = 249.1409.

Steady-State Enzyme Activity Assays. (*R*)-Methodol cleavage was measured at 29 °C in buffer A supplemented with 2.7 % acetonitrile as described previously.[12,16] Briefly, the formation of 6-MNA was monitored over time by absorption at 350 nm (ε_{350} = 5970 M^{-1} cm^{-1}). The enzyme concentration used was 1 µM for RA95.5-8 and 20 nM for RA95.5-8F. (*R*)-Methodol was synthesized as described previously,[12] and its concentration in the assay buffer (25 to 700 µM) was determined by absorption at 330 nm (ε_{330} = 1390 M^{-1} cm^{-1}) prior to initiating the reaction by addition of enzyme.

Methodol synthesis from acetone and 6-MNA was measured at 29 °C in buffer A by monitoring the consumption of 6-MNA spectroscopically (ε_{350} = 5970 M^{-1} cm^{-1} or ε_{370} = 1029 M^{-1} cm^{-1}). The enzyme concentration used was 5 µM for RA95.5-8 and 100 nM for RA95.5-8F. The concentration of acetone was kept constant at c = 1.0 M, whereas c(6-MNA) was varied (10 to 600 µM).

All measurements were performed in triplicate. The steady-state parameters k_{cat} and K_M were determined by fitting the data to the Michaelis-Menten equation. For the RA95.5-8-catalyzed synthesis of (*R*)-methodol, a modified equation was used to account for substrate inhibition by 6-MNA:

$$\frac{v_0}{[E]} = \frac{k_{cat} \cdot [S]}{K_M + [S] \cdot \left(1 + \frac{[S]}{K_i}\right)}$$

Kinetic Isotope Effects. KIEs were determined for both the cleavage and synthesis of (*R*)-methodol under steady-state conditions as described above by directly comparing the turnover of deuterated and non-deuterated substrates using the same enzyme batch. Deuterated d_5-(*R*)-methodol was used as the substrate for the cleavage experiment, whereas fully deuterated d_6-acetone and non-deuterated 6-MNA were used to determine the KIE for methodol synthesis. The KIE was calculated by the equation KIE = $k_{cat}(H)/k_{cat}(D)$. All measurements were performed in triplicate.

Single Turnover Enzyme Activity Assays. (*R*)-Methodol cleavage under single turnover conditions was measured at 29 °C in buffer A supplemented with 2.7 % acetonitrile using an Applied Photophysics SX18 stopped-flow spectrometer equipped with a xenon arc lamp. The formation of 6-MNA was monitored by fluorescence upon excitation at 330 nm and detection using a 400 nm cut-off filter. (*R*)-Methodol and enzyme (RA95.5-8 or RA95.5-8F) were mixed in a 1:5 ratio to give final concentrations of 150 µM (*R*)-methodol and 200 to 800 µM enzyme. An excess of enzyme over substrate and concentrations above K_D(substrate) were crucial to achieve single turnover conditions. The kinetic traces were collected in

triplicate, averaged and fitted to single exponential functions. The resulting single turnover rate constants k_{ST} were plotted against enzyme concentration.

6-MNA Binding Kinetics. 6-MNA binding to RA95.5-8 and RA95.5-8F was measured at 5 °C in buffer A supplemented with 2.7 % acetonitrile using an Applied Photophysics SX18 stopped-flow spectrometer equipped with a xenon arc lamp. Binding was monitored by a change in 6-MNA fluorescence with excitation at 330 nm and detection using a 400 nm cut-off filter. Enzyme (RA95.5-8 or RA95.5-8F) and 6-MNA were mixed in a 1:1 ratio to generate final concentrations of 5 µM enzyme and 15 to 70 µM 6-MNA. The kinetic traces were collected in triplicate, averaged and fitted to single exponential functions. The observed rate constants were linearly dependent on c(6-MNA), indicating a simple one-step binding mechanism. Thus, the association and dissociation rate constants, k_{on} and k_{off}, could be extracted from slope and y-axis intercept, respectively. Note that binding and release of 6-MNA are expected to be about 4-fold faster at 29 °C, the temperature used for all other kinetics experiments.

$^{16}O/^{18}O$ Isotope Exchange Kinetics by GC-MS. Oxygen isotope exchange in acetone was monitored using a Thermo Finnigan TRACE GC-MS instrument equipped with an Rtx-Wax column (30 m, RESTEK). Helium was used as the carrier gas (1.2 ml/min); the injection temperature was 250 °C; analysis temperature was constant at 100 °C; and the run time was 3 min. The enzyme was incubated with ^{16}O-acetone at 29 °C in buffer A containing 96 % $H_2{}^{18}O$. Samples (V = 1 µl) taken 1 min, 5 min and 9 min after starting the reaction were injected directly into the GC-MS, and the ratio of ^{16}O-acetone (m/z = 58) and ^{18}O-acetone (m/z = 60) was quantified. The measurements were performed at acetone concentrations of 10 to 500 mM and an enzyme concentration of 50 µM for RA95.5-8 and 500 nM for RA95.5-8F, respectively. The rate of background exchange, which was measured in the absence of enzyme, was subtracted before fitting the data to the Michaelis-Menten equation to determine k_{ex} and K_M(acetone) for Schiff base formation. All measurements were performed in triplicate.

Hydrogen/Deuterium Exchange Kinetics by NMR Spectroscopy. Hydrogen/deuterium exchange in acetone was monitored at 29 °C in buffer A using a 600 MHz Bruker Avance (UltraShield) NMR spectrometer equipped with a cryo probe. Two sets of experiments were performed: (i) The enzyme was incubated with h_6-acetone in D_2O buffer and the formation of mono-deuterated h_5,d_1-acetone was measured in a ^{1}H-NMR experiment; (ii) The enzyme was incubated with d_6-acetone in H_2O buffer and the formation of mono-protonated h_1,d_5-acetone was measured in a ^{2}H-NMR experiment. D_2O buffer was prepared by dissolving 358 mg HEPES and 526 mg NaCl in a final volume of 60 ml D_2O and adjusting to pD 7.5 using NaOD (note: pD = pH + 0.4). For the experiment performed in D_2O buffer, the enzyme was buffer-exchanged prior to measurement. The measurements were performed with acetone concentrations ranging from 25 to 500 mM. The enzyme concentration was 100 µM for RA95.5-8 and 3 µM for RA95.5-8F. $^1H/^2H$ spectra were collected every 10 min over the course of 2 hours (Figure S3/S4). Acetonitrile (200 mM) served as an internal standard for the integration of acetone peaks in all H/D exchange experiments. The kinetic data were fitted to the Michaelis-Menten equation to determine k_{ex} and K_M(acetone) for enamine formation.

ASSOCIATED CONTENT

Supporting Information

The Supporting Information is available free of charge on the ACS Publications website at DOI:

Additional kinetic, NMR and mass spectrometry data (PDF)

AUTHOR INFORMATION

Corresponding Author

*hilvert@org.chem.ethz.ch

Notes

The authors declare no competing financial interest.

ACKNOWLEDGMENT

We thank Professor Peter Chen and Armin Limacher for access to and technical support with the GC-MS. We are grateful to the NMR Service of the Laboratory of Organic Chemistry at ETH Zurich and Dr. Marc-Olivier Ebert and René Arnold in particular for performing the hydrogen/deuterium exchange experiments. We thank Professor Bernhard Jaun, Dr. Xavier Garrabou and Adrian Bunzel for helpful discussions and Duncan Macdonald for help with chiral HPLC. This work was generously supported by ETH Zurich and the Swiss National Science Foundation. C.Z. is recipient of a Marie Skłodowska-Curie Individual Fellowship (TIMEnzyme). R.Z. is grateful for a scholarship from the Stipendienfonds der Schweizerischen Chemischen Industrie (SSCI).

REFERENCES

(1) Kiss, G.; Celebi-Olcum, N.; Moretti, R.; Baker, D.; Houk, K. N. *Angew. Chem., Int. Ed.* **2013**, *52*, 5700-5725.

(2) Hilvert, D. *Annu. Rev. Biochem.* **2013**, *82*, 447-470.

(3) Rothlisberger, D.; Khersonsky, O.; Wollacott, A. M.; Jiang, L.; DeChancie, J.; Betker, J.; Gallaher, J. L.; Althoff, E. A.; Zanghellini, A.; Dym, O.; Albeck, S.; Houk, K. N.; Tawfik, D. S.; Baker, D. *Nature* **2008**, *453*, 190-195.

(4) Khersonsky, O.; Rothlisberger, D.; Dym, O.; Albeck, S.; Jackson, C. J.; Baker, D.; Tawfik, D. S. *J. Mol. Biol.* **2010**, *396*, 1025-1042.

(5) Khersonsky, O.; Kiss, G.; Rothlisberger, D.; Dym, O.; Albeck, S.; Houk, K. N.; Baker, D.; Tawfik, D. S. *Proc. Natl. Acad. Sci. U. S. A.* **2012**, *109*, 10358-10363.

(6) Blomberg, R.; Kries, H.; Pinkas, D. M.; Mittl, P. R.; Grutter, M. G.; Privett, H. K.; Mayo, S. L.; Hilvert, D. *Nature* **2013**, *503*, 418-421.

(7) Siegel, J. B.; Zanghellini, A.; Lovick, H. M.; Kiss, G.; Lambert, A. R.; St Clair, J. L.; Gallaher, J. L.; Hilvert, D.; Gelb, M. H.; Stoddard, B. L.; Houk, K. N.; Michael, F. E.; Baker, D. *Science* **2010**, *329*, 309-313.

(8) Preiswerk, N.; Beck, T.; Schulz, J. D.; Milovnik, P.; Mayer, C.; Siegel, J. B.; Baker, D.; Hilvert, D. *Proc. Natl. Acad. Sci. U. S. A.* **2014**, *111*, 8013-8018.

(9) Jiang, L.; Althoff, E. A.; Clemente, F. R.; Doyle, L.; Rothlisberger, D.; Zanghellini, A.; Gallaher, J. L.; Betker, J. L.; Tanaka, F.; Barbas, C. F., 3rd; Hilvert, D.; Houk, K. N.; Stoddard, B. L.; Baker, D. *Science* **2008**, *319*, 1387-1391.

(10) Althoff, E. A.; Wang, L.; Jiang, L.; Giger, L.; Lassila, J. K.; Wang, Z.; Smith, M.; Hari, S.; Kast, P.; Herschlag, D.; Hilvert, D.; Baker, D. *Protein Sci* **2012**, *21*, 717-726.

(11) Bjelic, S.; Kipnis, Y.; Wang, L.; Pianowski, Z.; Vorobiev, S.; Su, M.; Seetharaman, J.; Xiao, R.; Kornhaber, G.; Hunt, J. F.; Tong, L.; Hilvert, D.; Baker, D. *J. Mol. Biol.* **2014**, *426*, 256-271.

(12) Giger, L.; Caner, S.; Obexer, R.; Kast, P.; Baker, D.; Ban, N.; Hilvert, D. *Nat. Chem. Biol.* **2013**, *9*, 494-498.

(13) Agresti, J. J.; Antipov, E.; Abate, A. R.; Ahn, K.; Rowat, A. C.; Baret, J. C.; Marquez, M.; Klibanov, A. M.; Griffiths, A. D.; Weitz, D. A. *Proc. Natl. Acad. Sci. U. S. A.* **2010**, *107*, 4004-4009.

(14) Baret, J. C.; Miller, O. J.; Taly, V.; Ryckelynck, M.; El-Harrak, A.; Frenz, L.; Rick, C.; Samuels, M. L.; Hutchison, J. B.; Agresti, J. J.; Link, D. R.; Weitz, D. A.; Griffiths, A. D. *Lab Chip* **2009**, *9*, 1850-1858.

(15) Kintses, B.; Hein, C.; Mohamed, M. F.; Fischlechner, M.; Courtois, F.; Laine, C.; Hollfelder, F. *Chem. Biol.* **2012**, *19*, 1001-1009.

(16) Obexer, R.; Godina, A.; Garrabou, X.; Mittl, P. R.; Baker, D.; Griffiths, A. D.; Hilvert, D. *Nat. Chem.* **2017**, *9*, 50-56.

(17) Gefflaut, T.; Blonski, C.; Perie, J.; Willson, M. *Prog. Biophys. Mol. Biol.* **1995**, *63*, 301-340.

(18) Windle, C. L.; Muller, M.; Nelson, A.; Berry, A. *Curr. Opin. Chem. Biol.* **2014**, *19*, 25-33.

(19) Garrabou, X.; Beck, T.; Hilvert, D. *Angew. Chem., Int. Ed.* **2015**, *54*, 5609-5612.

(20) Garrabou, X.; Wicky, B. I.; Hilvert, D. *J. Am. Chem. Soc.* **2016**, *138*, 6972-6974.

(21) Garrabou, X.; Macdonald, D. S.; Hilvert, D. *Chemistry* **2017**, *23*, 6001-6003.

(22) Lassila, J. K.; Baker, D.; Herschlag, D. *Proc. Natl. Acad. Sci. U. S. A.* **2010**, *107*, 4937-4942.

(23) Model, P.; Ponticorvo, L.; Rittenberg, D. *Biochemistry* **1968**, *7*, 1339-1347.

(24) Biellmann, J. F.; O'Connell, E. L.; Rose, I. A. *J. Am. Chem. Soc.* **1969**, *91*, 6484-6488.

(25) Pratt, R. F. *Biochemistry* **1977**, *16*, 3988-3994.

(26) Rose, I. A.; Warms, J. V. *Biochemistry* **1985**, *24*, 3952-3957.

(27) Rose, I. A.; Warms, J. V.; Kuo, D. J. *J. Biol. Chem.* **1987**, *262*, 692-701.

(28) Shulman, A.; Sitry, D.; Shulman, H.; Keinan, E. *Chemistry* **2002**, *8*, 229-239.

(29) Schurmann, M.; Sprenger, G. A. *J. Biol. Chem.* **2001**, *276*, 11055-11061.

(30) Thorell, S.; Schurmann, M.; Sprenger, G. A.; Schneider, G. *J. Mol. Biol.* **2002**, *319*, 161-171.

(31) Tittmann, K. *Bioorg. Chem.* **2014**, *57*, 263-280.

(32) Schneider, S.; Sandalova, T.; Schneider, G.; Sprenger, G. A.; Samland, A. K. *J. Biol. Chem.* **2008**, *283*, 30064-30072.

(33) Sautner, V.; Friedrich, M. M.; Lehwess-Litzmann, A.; Tittmann, K. *Biochemistry* **2015**, *54*, 4475-4486.

(34) Boyken, S. E.; Chen, Z.; Groves, B.; Langan, R. A.; Oberdorfer, G.; Ford, A.; Gilmore, J. M.; Xu, C.; DiMaio, F.; Pereira, J. H.; Sankaran, B.; Seelig, G.; Zwart, P. H.; Baker, D. *Science* **2016**, *352*, 680-687.

(35) Patrick, W. M.; Firth, A. E. *Biomol. Eng.* **2005**, *22*, 105-112.

(36) Kazlauskas, R. J.; Bornscheuer, U. T. *Nat. Chem. Biol.* **2009**, *5*, 526-529.

(37) Kille, S.; Acevedo-Rocha, C. G.; Parra, L. P.; Zhang, Z. G.; Opperman, D. J.; Reetz, M. T.; Acevedo, J. P. *ACS Synth. Biol.* **2013**, *2*, 83-92.

(38) Fallah-Araghi, A.; Baret, J. C.; Ryckelynck, M.; Griffiths, A. D. *Lab Chip* **2012**, *12*, 882-891.

(39) Fischlechner, M.; Schaerli, Y.; Mohamed, M. F.; Patil, S.; Abell, C.; Hollfelder, F. *Nat. Chem.* **2014**, *6*, 791-796.

(40) Chen, B.; Lim, S.; Kannan, A.; Alford, S. C.; Sunden, F.; Herschlag, D.; Dimov, I. K.; Baer, T. M.; Cochran, J. R. *Nat. Chem. Biol.* **2016**, *12*, 76-81.

Table of Contents artwork